

SYNTHESIS AND EVALUATION OF MAGNETIC ZEOLITE NANO-COMPOSITE FOR REMOVAL OF RU FROM AQUEOUS SOLUTIONS

Leila Eskandari^{1*}, Farshad Kheiri¹, Mozhgan Irawani², Mohammad Sirousazar¹

¹ Faculty of Chemical Engineering, Urmia University of Technology, Urmia, Iran

² Faculty of Chemistry, University of Isfahan, 81746-73441 Isfahan, Iran

Received September 17, 2018; Accepted October 14, 2018

Abstract

Ruthenium compounds are distinctly toxic and carcinogenic, and its treatment has received much attention. Within the present studies, a singular magnetic nano zeolite composite (MZNC) became organized. Natural clinoptilolite tuff changed into nanoparticles by the use of a mechanical technique. The samples had been carried out to signify the adsorbents by XRD, XRF, FT-IR, DTG, SEM, and VSM. The nanocomposites were evaluated for Ruthenium (Ru) removal from aqueous solutions. The outcomes of the analytical variables, inclusive of pH, preliminary ion concentration, contact time, and temperature have been investigated. The saturation magnetization of the nano-composite turned into measured as 19.50 emu g^{-1} through which the magnetic separations of the samples have been facilitated after the adsorption procedure. The thermodynamic values of ΔG° and ΔH° represented the endothermic and spontaneous natures of Ru elimination.

Keywords: *Magnetic nanocomposite, Nano clinoptilolite, Ruthenium, Isotherm.*

1. Introduction

The environmental effect of the release of poisonous and radioactive pollutions from the nuclear industry has brought about a wide kind of studies on the removal of such pollutants. Therefore, to protect human health and the surroundings from risks resulting from radioactive waste and to keep away from any undue burden on future generations, radioactive waste needs to be controlled responsibly. Ion exchange process is one of the most effective approaches to the remedy of heavy metals [1-5]. Amongst distinct ion exchangers zeolites have received considerable attention for contaminant removal owing to their high exchange capacity, low cost and worldwide abundance [6-10]. Considering the largescale utilizations, natural zeolites seem more ascendant than synthetic ones, due to their low cost, abundant and much less chemical pollutants during production [11]. In comparison to the micro-sized zeolites, nano-crystalline zeolites have greater ion-exchange abilities, quicker exchange kinetics, larger surface areas, and more adjustable porosities. Yet, in spite of these advantages, separating them from the medium is the main challenge. This can be coped with by using magnetic separation technique. By applying nano-magnetic composites, these new methods open a simpler, faster, and more accurate way to the removal of elements [12]. Despite the fact that different methods have been reported for the synthesis of nano zeolites, as an alternative technique, the zeolite particle size may be decreased mechanically using particularly designed ball mills [13-17]. In spite of these advantages, separation of ion exchangers with the particle size in nanoscale from the medium is very difficult. This problem could be overcome by using a magnetic separation technique. This technique facilitates nano zeolite separation from solution in synthesis and usage steps since magnetic composites can be separated by efficient, simple, and fast magnetic separation process. For this kind of separation, extensive researches have been performed. The present study, magnetic nanocomposite was synthesized and characterized for studying their efficiencies of Ru removal from aqueous solutions. Meanwhile, the

effects of varied parameters, including pH, initial ion concentration, contact time, and temperature were evaluated and 4 optimized. Moreover, for the experimental data assessment, different kinetic and isotherm models were employed.

2. Experimental procedure

2.1. Reagents and methods

All the chemical reagents used in this study were of analytical reagent grade [AR Grade]. $\text{FeCl}_3 \cdot 6\text{H}_2\text{O}$ (Aldrich 98%), $\text{FeCl}_2 \cdot 4\text{H}_2\text{O}$ (Aldrich 99%), and ammonium hydroxide (Aldrich 28–30% of ammonia) were applied for magnetic particle preparation, and Ru ions were supplied as ruthenium trichloride hydrate (also from Merck, Darmstadt, Germany). The natural clinoptilolite tuff belonged to Semnan region in the north-east of Iran. Identifications of the structural phases of the nanocomposite were achieved by usage of a Bruker D8 Advance X-ray diffractometer. The chemical compositions of the samples were determined through PANalytical Magix XRF spectrometry. An IR Prestige-21 Model spectrophotometer (Shimadzu, Japan) was utilized to obtain FT-IR spectra. Thermo-Gravimetric Analysis (TGA) of the samples was performed using a Mettler TG-50 Thermal Analyzer with a heating rate of $10^\circ\text{C min}^{-1}$. A vibrating sample magnetometer (Meghnatis Daghigh Kavir Company, Iran) was used to characterize MZNC magnetic properties. A Philips EM-208S transmission electron microscope was utilized to take the relevant images. Also, ICP-AES technique (Integra XL by GBC Australia) was employed to specify Ru concentration. The prepared nanocomposite was separated with the aid of a permanent magnet. Finally, the product was washed four times with deionized–deoxygenated water and then dried at 50°C for 5 h. The nanocomposite was prepared by adding the amount of nano zeolite clinoptilolite Fig. 1.

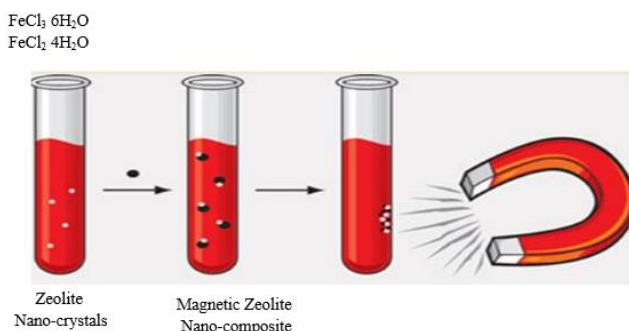


Fig. 1. Scheme of synthesis procedure of the nanocomposite

2.2. Adsorption experiments

The adsorption of Ru was studied by a batch technique to discover the optimum conditions. A sample of 0.05 g of nano zeolite or nanocomposite was equilibrated with 10 mL of Ru solution of known concentration at the fixed temperature for a known period of time. After equilibration, filtration of the solid phase was followed by centrifugation of the filtrate (3000 rpm for 5 min) while the nano-composite separation from liquid phase was followed with efficient, simple, and fast filtering. 10 mL of the supernatant solution was then taken for Ru measurement. The adsorbed amount of Ru was calculated from the difference in concentrations before and after adsorption.

$$q = (C_i - C_f) \times V/m \quad (1)$$

where q is the adsorbed amount of metal ions by a unit mass of zeolite (meq g^{-1}); C_i and C_f are the initial and final Ru concentrations (meq L^{-1}), respectively; m is the used amount of zeolite (g), and V is the volume of Ru solution (L). The effects of different parameters, which is included initial Ru concentration, the solution pH, the contact time, and the temperature were investigated.

3. Results and discussion

3.1. Characterization of M ZNC

The XRD patterns of raw nano-clinoptilolite (NCP) and magnetite zeolite nano-composite (MZNC) are shown in Figure 2. The characteristic lines at 2θ values of 10.1° , 11.4° , 17.3° , 23° , 26° , 28.2° , 30.2° , 32° , 35° , 37° and 39° in the pattern (a) can be attributed to clinoptilolite crystalline structure data [18]. This confirms that the sample used in this work has a typical clinoptilolite phase as the microporous component. The diffraction line of iron oxide was observed at 2θ values of 35.9° , 42° and 73° in the XRD pattern of MZNC sample (b) shows the formation of iron oxide in the zeolite structure [19]. The relative line intensity and line position related to zeolite clinoptilolite remained unchanged, which represented that the crystal structure of zeolite had been stable during the preparation of composite. Through Scherrer's equation [20], the magnetite particle size of the composite was appeared to be 22.4 nm.

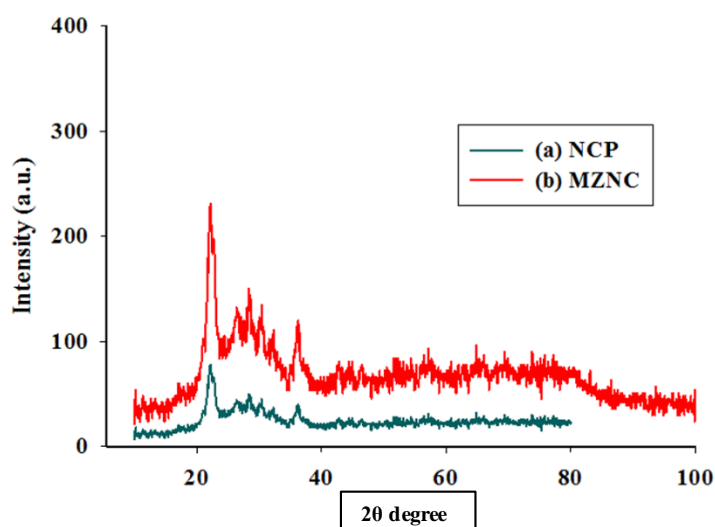


Fig 2. XRD patterns of the nano zeolite (matched with a reference pattern of clinoptilolite) (a), and MZNC (b)

Zeolite and MZNC chemical compositions (Table 1) were obtained by the XRF method. The composite consisted of 19.86 wt.% Fe_2O_3 . The Si/Al ratio of the present zeolite sample was 4.85, which was consistent with the previous findings placing the ratio within a range of 4-5.5 [21]. The sum of the exchangeable ions estimated Theoretical Cation Exchange Capacity (TCEC), Na^+ , K^+ , Ca^{2+} , and Mg^{2+} in the zeolite included. The disparity between TCEC and Cation Exchange Capacity (CEC) (Table 1) was owing to the fact that some counter-ion sites in the zeolite particles were not available for cation exchange.

Table 1. Chemical compositions of zeolite and MZNC obtained through XRF analysis

	SiO ₂	Al ₂ O ₃	Na ₂ O	TiO ₂	K ₂ O	CaO	MgO
CLI	67.41	11.82	2.66	0.10	2.44	1.31	0.71
MZNC	53.21	9.28	1.92	1.096	1.48	1.25	0.71
	SrO	Fe ₂ O ₃	LOI ^a	Total	Si/Al	TCEC ^c	CEC ^c
CLI	0.13	1.32	11.46	99.54	4.85	1.736	1.561
MZNC	n.d. ^b	19.86	12.01	99.81	4.87	1.335	1.218

CLI-clinoptilolite; ^a Loss on ignition; ^b Not detected; ^c (meq g⁻¹)

The FT-IR spectra of the samples, zeolite, and composite, were reported under a range of 400-4000 cm^{-1} (Fig. 3). Absorption bands of water at 1638 cm^{-1} in the range of 3000-3600 cm^{-1} confirmed significant hydrations of the zeolite. The band at 1070 cm^{-1} was attributed to the

asymmetric stretching vibration modes of the internal T-O bonds in TO₄ tetrahedra (T=Si and Al). The 609 and 465 cm⁻¹ bands risen from the stretching vibration modes of O-T-O groups and the vibration modes of bending of T-O bonds, respectively [22]. About the zeolite, the regions corresponding to (Si-O and Al-O) and (O-Si-O and O-Al-O) showed strong bands, which indicate an increase within the surface areas and aluminosilicate bonds of the zeolite. The characteristically related band to Fe-O-Fe bond of iron oxide must have appeared at 584 cm⁻¹ [19].

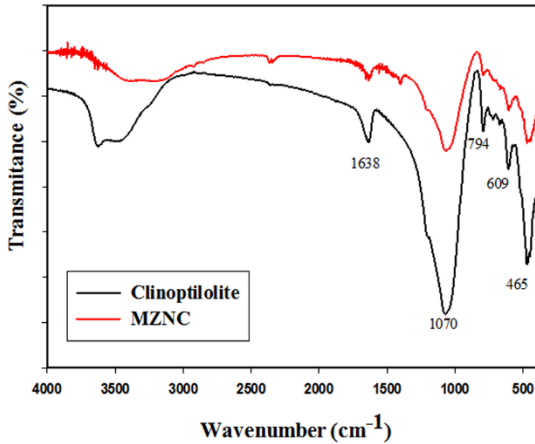


Figure 3. FTIR spectra of clinoptilolite and MZNC

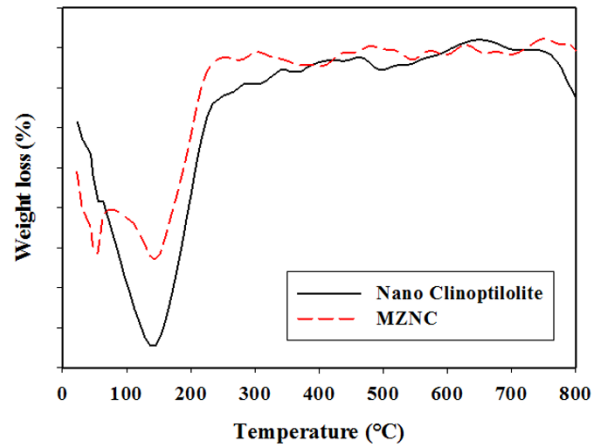
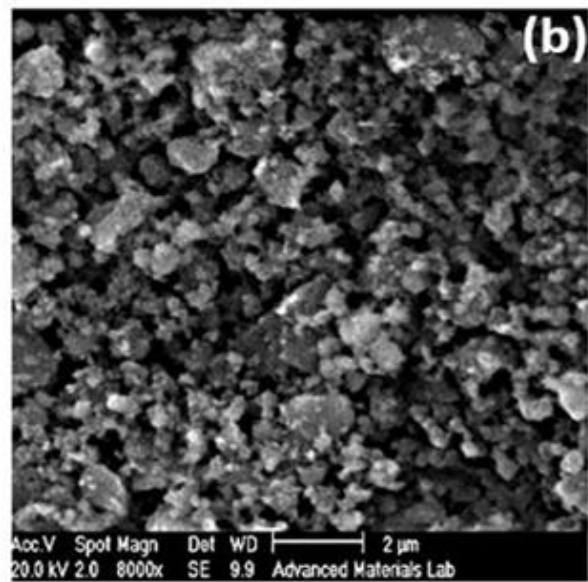
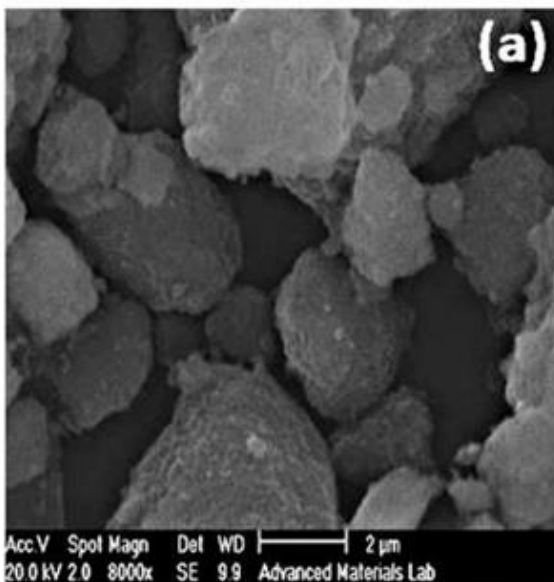


Figure 4. DTG curves of Nano clinoptilolite and MZNC

In the DTG curves of the nano-zeolite clinoptilolite and MZNC, two weight-loss peaks occurring between 50°C and 120°C were assigned to the loss of the adsorbed water Fig. 4. After 280°C, the adsorbents exhibited no dehydration peaks up to 800°C, which means that the samples were thermally stable.

The disparity between the amorphous surface structures of the sample of natural zeolite and nano-zeolite clinoptilolite with a uniform surface was visible in accordance with SEM images Fig 5 (a and b). Owing to the scarcity of monotony and extensive range of particle dimensions, determination of the particle size distribution not be able to accurately carried out for micro-sized clinoptilolite, according to (Fig. 5a), but for nano-sized particles given in Fig 5b. Also, TEM images illustrated iron oxide particles to have been nano-sized and bound to the aluminosilicate framework of nano-zeolite (Fig 5c).



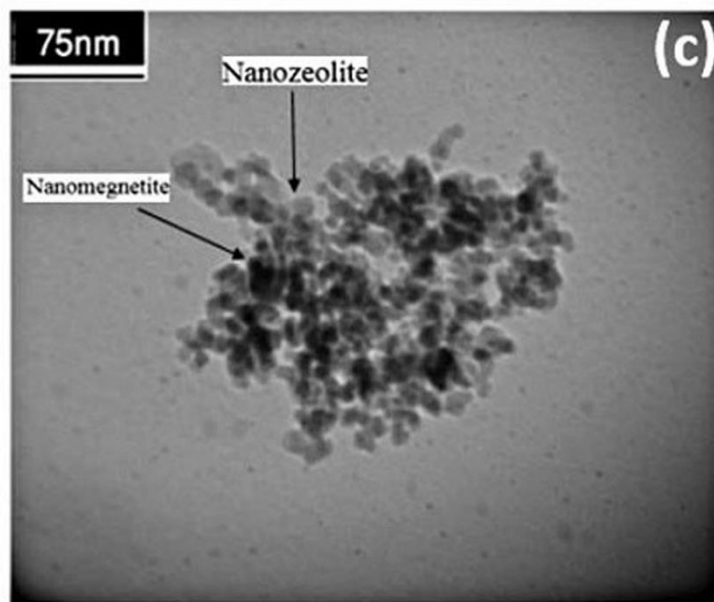


Figure 5 (a, b). SEM images of zeolite clinoptilolite (a) and nano clinoptilolite (b).

Figure 5 (c). The MZNC TEM images

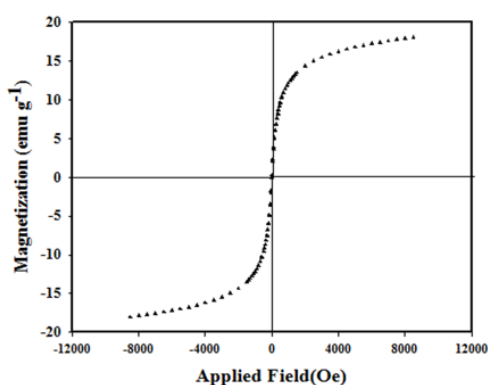


Figure 6. The hysteresis loops of MZNC

This new composite's feature was its magnetic property, which means that it was characterized by a sample of the vibrating magnetometer in this study Fig 6. The magnetic curve illustrated no hysteresis loop and remanence, which indicate the good super-paramagnetic properties of MZNC. The zero amount of remanence certified that the composite had not retained magnetization after being exposed to an external magnetic field and they could be thus re-dispersed after removing the magnetic field. Nanocomposite exhibited the saturation magnetizations of approximately 19.50 emu g^{-1} at 298K. This value verified the adequate magnetic properties of MZNC to be appealed by a permanent magnet.

3.2. Optimization of conditions

3.2.1. Effect of pH

The adsorption of Ru species was at its greatest at pH 2 (Figure. 7), so the present adsorption studies were performed at that pH. The study of electrochemical and spectral on RuCl_3 in aqueous solution in the pH of 0.4-2.0 have shown that Ru (III) may exist as four major species, $[\text{RuCl}_4(\text{H}_2\text{O})_2]$, $[[\text{RuCl}_3(\text{H}_2\text{O})_3]$, $[\text{RuCl}_2(\text{H}_2\text{O})_4]^+$, and/or $[\text{RuCl}(\text{H}_2\text{O})_5]^{2+}$. They are referred to here as species 1, 2, 3, and 4, respectively. At pH 2, only species 3 was present [23]. The charge repulsion between the zeolite surface and negatively charged species of Ru at $\text{pH} < 2.0$ may be one of the reasons for poor adsorption at these pH values. Competition with H_3O^+ is another possible reason. At higher pH values, hydroxyl ions are introduced gradually to the coordination sphere and negatively charged Ru complexes are produced.

3.2.2. Effect of contact time

The results show that as contact time increased, Ru adsorption increased initially, but then approached a constant value rapidly (Figure. 8). Equilibrium was attained after 24 h, after

which time no further significant increase occurred in the level of adsorption. After just 15 h, 92% of the adsorption amount at equilibrium had been achieved. A shaking time of 24 h employed for all of the equilibrium adsorption studies was sufficient to ensure that adsorption equilibrium was reached.

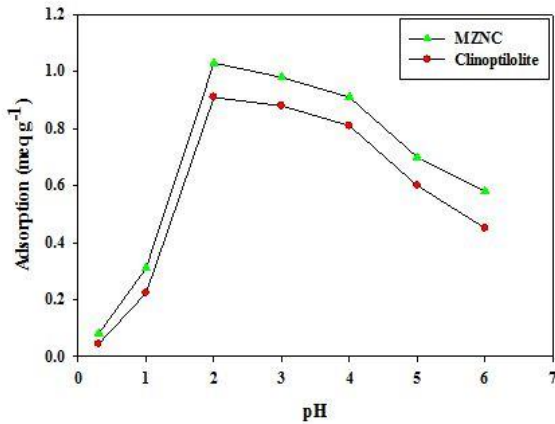


Figure 7. pH effect on sorption of Ru

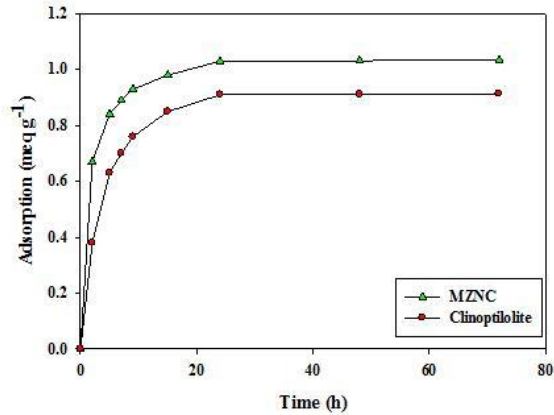


Figure 8. Contact time effect on adsorption of Ru onto clinoptilolite and MZNC

3.3. Adsorption kinetics and thermodynamics

The kinetics of adsorption was evaluated by applying four different models including the pseudo-first-order equation, the pseudo-second-order equation, Elovich equation, and intra-particle diffusion model. These models were tested to fit experimental data obtained by batch experiments.

The pseudo-first-order equation is generally expressed as follows:

$$\ln (q_e - q_t) = \ln q_e - k_1 t \tag{2}$$

where q_e and q_t are the ions adsorbed amount per unit mass of the adsorbent at equilibrium and at any time t , respectively and k_1 is the rate constant of pseudo-first-order sorption (min^{-1}).

The values of k_1 and q_e were regulated from the slope and the intercept of plotting of $\log (q_e - q_t)$ vs. t . The results are listed in Table. 2. Although no extremely low values were obtained for R2, the calculated q_e was not consistent with that of experimental data. Hence, the adsorption process did not follow a pseudo-first-order model. The linear form of the pseudo-second-order kinetic model is written as follow:

$$t/q_t = 1/(k_2 q_e^2) + (1/q_e)t \tag{3}$$

The initial sorption rate can be calculated by the following formula:

$$h = k_2 q_e^2 \tag{4}$$

where k_2 is the rate constant of pseudo-second-order kinetic sorption (g/mg/min). The calculated values of k_2 , q_e , and h values and the correlation coefficients (R2) are listed in table 2. The comparison of k_2 values indicated faster ion adsorption onto MZNC is faster than on clinoptilolite.

Table 2. Kinetic parameters of pseudo-first-order and pseudo-second-order kinetic models

sorbents	q_e (exp.) ($\times 10^{-1}$) (meqg ⁻¹)	pseudo-first-order model			pseudo-second-order model			
		k_1 ($\times 10^{-1}$) (h ⁻¹)	q_e (theor.) ($\times 10^{-1}$) (meqg ⁻¹)	R ²	k_2 (meq ⁻¹ h ⁻¹)	q_e ($\times 10^{-1}$) (meq g ⁻¹)	h ($\times 10^{-1}$) (meq g ⁻¹ h ⁻¹)	R ²
Clinoptilolite	9.1	1.775	77.49	0.9868	0.4695	9.4993	4.2366	0.9994
MZNC	10.3	1.881	63.02	0.9132	0.8468	10.5407	9.4085	0.9999

3.3.1. Sorption thermodynamics

The effect of sorption temperature on Ru removal was investigated at five different temperatures. The adsorption capacity enhanced with increasing temperature (Fig 9). The thermodynamic parameters, including enthalpy change (ΔH°) and entropy change (ΔS°), can be obtained using the Van't Hoff equation.

$$\ln K_d = - (\Delta H^\circ/RT) + (\Delta S^\circ/R) \tag{5}$$

A plot of $\ln K_d$ vs. $1/T$ is shown in Fig 10. The free energy change of the adsorption (ΔG°) is calculated as follows:

$$\Delta G^\circ = \Delta H^\circ - T\Delta S^\circ \tag{6}$$

The calculated thermodynamic parameters are summarized in Table 3. Since ΔH° values are positive, the adsorption process is endothermic in nature.

Table 3. Thermodynamic parameters of Ru adsorption

Sorbent	ΔH° (kJ/mol)	ΔS° (kJ/mol/K)	ΔG° (kJ/mol)			
			298(K)	313(K)	328(K)	343(K)
CLI	2.312	29.74	-6.55	-6.99	-7.44	-7.88
MZNC	3.744	30.99	-5.49	-5.95	-6.42	-6.88

CLI- clinoptilolite

The positive values of ΔS° suggested that the randomness at the solid/solution interface had increased during the sorption process. The negative values of ΔG° indicated that Ru adsorption reaction was spontaneous. The decrease in ΔG° values with increasing temperature showed that the spontaneous nature of sorption was directly proportional to temperature. Therefore, the adsorption process was favored when the temperature was augmented. The greater absolute values of ΔG° for MZNC compared to clinoptilolite revealed that the adsorption of the former on Ru had been more favored.

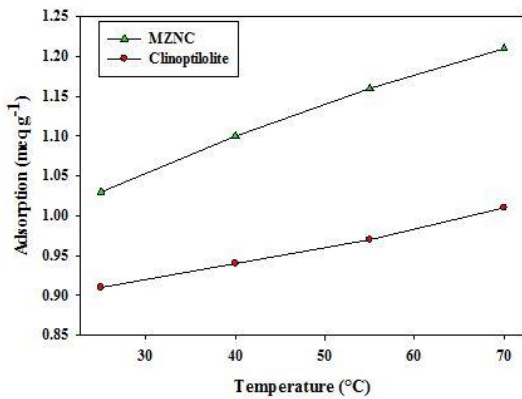


Figure 9. Temperature effect on Ru adsorption onto clinoptilolite and MZNC

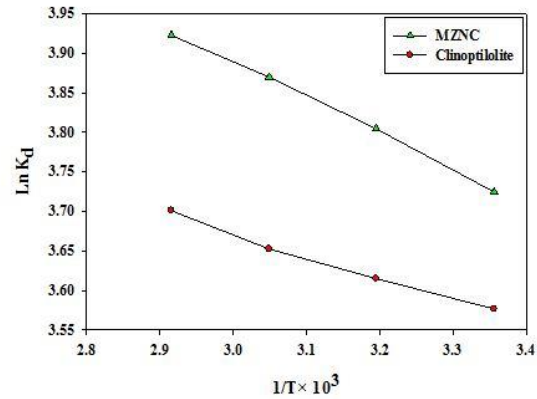


Figure 10. Van't Hoff plot for adsorption of Ru

3.3.2. Sorption isotherm

To investigate the effect of initial concentration, various concentrations of Ru solution were equilibrated with constant amounts of the adsorbents (Fig 11). The initial fast adsorption was followed by a slow approach to equilibrium at a higher concentration. Three isotherm models, including Langmuir, Freundlich, and Dubinin-Radushkviech (D-R) models were employed to examine the experimental data.

3.3.3. Langmuir isotherm model

Langmuir isotherm assumes that the sorption occurs at specific homogeneous sites within the adsorbent. This model is expressed by:

$$C_e/q_e = 1/(Q_0b) + C_e/Q_0 \tag{7}$$

where Q_0 denotes the saturation adsorption capacity (mg/g), and b represents the Langmuir constant related to the free energy of adsorption calculated from the slope and intercept (Table 4). The plot of C_e/q_e vs. C_e is shown in Fig 12. The important parameter of Langmuir isotherm is the dimensionless constant, RL , which can be calculated as follows:

$$R_L = 1 / (1 + bC_0) \tag{8}$$

where C_0 stands for the highest initial metal ion concentration (mg/L).

Table 4. Adsorption isotherm parameters for Ru adsorption

Isotherm	Sorbent	Model parameters			
		Q_0 (mg/g)	$b \times 10^3$ (L/mg)	$RL \times 10^3$	R^2
Langmuir	Clinoptilolite	131.4	19.849	0.01	0.7812
	MZNC	405.5	43.759	0.045	0.9998
		Model parameters			
Freundlich	Sorbent	n	K_f (mg/g)	R^2	
Freundlich	Clinoptilolite	0.152	262.84	0.9524	
	MZNC	0.336	928.53	0.9644	
		Model parameters			
D-R	Sorbent	$\beta \times 10^{-9}$ (mol ² /kJ ²)	q_m (mmol/g)	E (kJ/mol)	R^2
D-R	Clinoptilolite	6.38	2.974	12.7	0.9970
	MZNC	8.45	3.126	16.0	0.9530

The values of this parameter indicate the unfavorable ($RL > 1$), linear ($RL = 1$), favorable ($0 < RL < 1$), and irreversible ($RL = 0$) types of the adsorption isotherm.

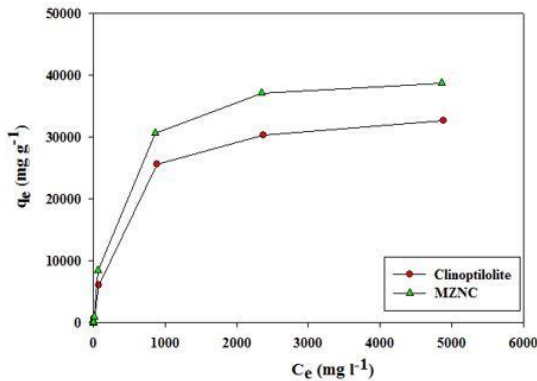


Figure 11. Different initial ion concentration effect on Ru adsorption onto clinoptilolite and MZNC

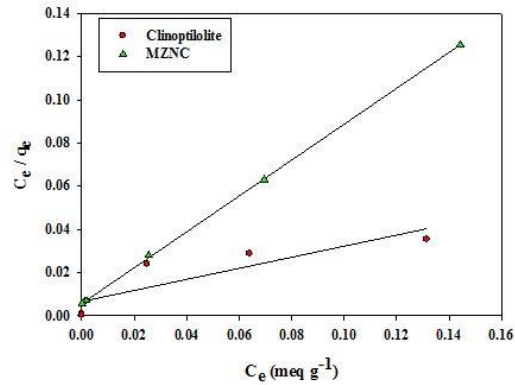


Figure 12. Langmuir isotherm plots for adsorption of Ru onto clinoptilolite and MZNC

3.3.4. Freundlich isotherm model

Freundlich isotherm model makes the assumption that multi-layer sorption occurs at a heterogeneous surface. This model was used to estimate the intensity of the adsorption process and the relative sorption capacity. A linear form of the Freundlich equation is shown as follows:

$$\log q_e = \log K_f + 1/n \log C_e \tag{9}$$

where K_f denotes the Freundlich constant relevant to the adsorbent capacity, and n displays the constant related to the intensity of the adsorption process.

The Freundlich isotherm is shown in Fig 13, and their constants are represented in Table 4. The Freundlich constant (n) was greater than its unity, indicating that an increasing tendency of the adsorption process had occurred with the elevation of ion concentration. K_f value of MZNC was higher compared to clinoptilolite, corroborating a greater adsorption tendency of the adsorbents towards MZNC.

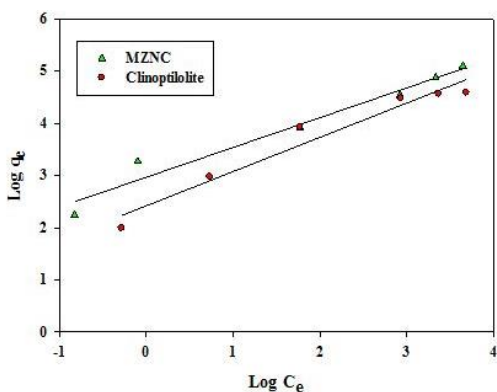


Figure 13. Freundlich isotherm plots for adsorption of Ru onto clinoptilolite and MZNC

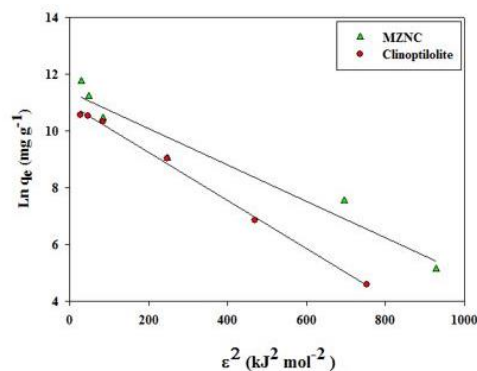


Figure 14. D-R isotherm plots for adsorption of Ru onto clinoptilolite and MZNC

3.3.5. Dubinin–Radushkviech isotherm model

D–R isotherm was used to distinguish between the physical and chemical adsorptions of the ions and estimate the apparent free energies of adsorption. The related equation is given as follows:

$$\ln q_e = \ln q_m - \beta \varepsilon^2 \quad (10)$$

where q_m is the maximum adsorption capacity (mequiv/g), b is the D–R constant related to the sorption energy ($\text{mol}^2/\text{K/J}^2$), and e is the Polanyi potential:

$$\varepsilon = RT \ln(1 + 1/C_e) \quad (11)$$

where R is the gas constant ($\text{kJ}\cdot\text{mol}^{-1}\cdot\text{K}$), and T is the absolute temperature (K).

The D–R isotherm is plotted in Fig. 14 and the obtained parameters are represented in Table 5. In a solution, when 1 mol of an ion is transferred to the surface of an adsorbent from infinity, its free energy is called the mean energy of adsorption (E), which is calculated as follows:

$$E = (2\beta)^{-1/2} \quad (12)$$

The magnitude of E within a range of 8–16 kJ/mol demonstrates that the sorption process is done through an ion exchange interaction. The reaction mechanism can be related to the magnitude of E . When E value is within the range of 8–16 kJ/mol, the sorption process is followed by ion exchange, but when $E < 8.0$ kJ/mol, physical forces are responsible for the process [25].

4. Conclusion

The magnetite-zeolite nano- composite was synthesized, characterized, and evaluated for Ru removal from aqueous solutions. The nano-composite represented a high cation exchange capacity, high selectivity towards Ru, and rapid adsorption kinetics as compared to the zeolite itself. The nano-composite displayed a 34.9% increase in adsorption capacity. The results of the kinetic studies suggested that the initial sorption rate and rate constant were greater when using the nano-composite instead of the zeolite. The VSM results verified the sufficient magnetic strengths of the nanocomposite to be attracted by a magnetic field. The Pseudo-Second Order model gave a better correlation with the experimental kinetic data compared to the pseudo-first-order model, confirming the dominant process of the chemical sorption. The values of the thermodynamic parameters demonstrated the endothermic and spontaneous natures of the adsorption process.

References

- [1] Sharma P, Sharma M, Tomar R. Na-HEU zeolite synthesis for the removal of Th (IV) and Eu (III) from aqueous waste by a batch process. *Journal of the Taiwan Institute of Chemical Engineers*. 2013; 44(3):480–8.
- [2] Mohseni-Bandpi A, Al-Musawi TJ, Ghahramani E, Zarrabi M, Mohebi S, Vahed SA. Improvement of zeolite adsorption capacity for cephalixin by coating with magnetic Fe₃O₄ nanoparticles. *Journal of Molecular Liquids*. 2016; 218: 615–24.

- [3] Ltaief OO, Siffert S, Fourmentin S, Benzina M. Synthesis of Faujasite type zeolite from low grade Tunisian clay for the removal of heavy metals from aqueous waste by batch process: Kinetic and equilibrium study. *Comptes Rendus Chimie*. 2015; 18(10):1123-33.
- [4] Gupta P, Khanday WA, Majid SA, Kushwa V, Tomar SS, Tomar R. Study of sorption of metal oxoanions from waste water on surfactant modified analog of laumontite. *Journal of Environmental Chemical Engineering*. 2013; 1(3):510-5.
- [5] Kabiri-Tadi M, Faghihian H. Removal of ruthenium from aqueous solution by clinoptilolite. *Clays and Clay Minerals*. 2011; 59(1):34-41.
- [6] Kong S, Wang Y, Zhan H, Yuan S, Yu M, Liu M. Adsorption/oxidation of arsenic in groundwater by nanoscale Fe-Mn binary oxides loaded on zeolite. *Water Environment Research*. 2014; 86(2):147-55.
- [7] Moamen OA, Ismail IM, Abdelmonem N, Rahman RA. Factorial design analysis for optimizing the removal of cesium and strontium ions on synthetic nano-sized zeolite. *Journal of the Taiwan Institute of Chemical Engineers*. 2015; 55:133-44.
- [8] Noli F, Buema G, Misaelides P, Harja M. New materials synthesized from ash under moderate conditions for removal of toxic and radioactive metals. *Journal of Radioanalytical and Nuclear Chemistry*. 2015; 303(3):2303-11.
- [9] Cretescu I, Soreanu G, Harja M. A low-cost sorbent for removal of copper ions from wastewaters based on sawdust/fly ash mixture. *International Journal of Environmental Science and Technology*. 2015; 12(6):1799-810.
- [10] De Haro-Del Rio DA, Al-Joubori S, Kontogiannis O, Papadatos-Gigantes D, Ajayi O, Li C, Holmes SM. The removal of caesium ions using supported clinoptilolite. *Journal of hazardous materials*. 2015; 289:1-8.
- [11] Nezamzadeh-Ejhieh A, Salimi Z. Heterogeneous photodegradation catalysis of o-phenylenediamine using CuO/X zeolite. *Applied Catalysis A: General*. 2010; 390(1-2):110-8.
- [12] Song W, Li G, Grassian VH, Larsen SC. Development of improved materials for environmental applications: Nanocrystalline NaY zeolites. *Environmental science & technology*. 2005; 39(5):1214-20.
- [13] Charkhi A, Kazemian H, Kazemini M. Optimized experimental design for natural clinoptilolite zeolite ball milling to produce nano powders. *Powder technology*. 2010; 203(2):389-96.
- [14] Chu X, Li X, Dong Y, Qiao H, Bai L. Preparation of Nano-SnO₂ Abrasives and Their Application in Chemical Mechanical Polish of Ruthenium. *Rare Metal Materials and Engineering*. 2013; 42(4):692-5.
- [15] Patra D, Chaaban AH, Darwish S, Saad HA, Nehme AS, Ghaddar TH. Time resolved study of three ruthenium (II) complexes at micellar surfaces: A new long excited state lifetime probe for determining critical micelle concentration of surfactant nano-aggregates. *Colloids and Surfaces B: Biointerfaces*. 2016; 138: 32-40.
- [16] Nezamzadeh-Ejhieh A, Raja G. Modification of nanoclinoptilolite zeolite with hexadecyltrimethylammonium surfactant as an active ingredient of chromate-selective membrane electrode. *Journal of chemistry*. 2013.
- [17] Nezamzadeh-Ejhieh A, Zabihi-Mobarakeh H. Heterogeneous photodecolorization of mixture of methylene blue and bromophenol blue using CuO-nano-clinoptilolite. *Journal of Industrial and Engineering Chemistry*. 2014; 20(4): 1421-31.
- [18] Maity D, Agrawal DC. Synthesis of iron oxide nanoparticles under oxidizing environment and their stabilization in aqueous and non-aqueous media. *Journal of Magnetism and Magnetic Materials*. 2007; 308(1): 46-55.
- [19] Klug HP, Alexander LE. X-ray diffraction procedures: for polycrystalline and amorphous materials. *X-Ray Diffraction Procedures: For Polycrystalline and Amorphous Materials*, 2nd Ed, Wiley-VCH 1974; P.992.
- [20] Breck DW. Zeolite molecular sieves: structure, chemistry and use. Krieger; 1984.
- [21] Jacobs PA, Flanigen EM, Jansen JC, van Bekkum H. Introduction to zeolite science and practice. Elsevier; 2001 Jun 26.
- [22] Taqui Khan MM, Ramachandraiah G, Rao AP. Ruthenium (III) chloride in aqueous solution: electrochemical and spectral studies. *Inorganic Chemistry*. 1986; 25(5): 665-70.
- [23] Mohan D, Chander S. Single, binary, and multicomponent sorption of iron and manganese on lignite. *Journal of Colloid and Interface Science*. 2006; 299(1): 76-87.
- [24] Helfferich FG, Dranoff JS. Ion Exchange. McGraw-Hill, New York. 1962: P.624.

To whom correspondence should be addressed: Leila Eskandari, Faculty of Chemical Engineering, Urmia University of Technology, Urmia, Iran